International Journal of Mass Spectrometry 303 (2011) 118–124

Contents lists available at ScienceDirect

International Journal of Mass Spectrometry

journal homepage: www.elsevier.com/locate/ijms

Real time bipolar time-of-flight mass spectrometer for analyzing single aerosol particles

Lei Li[a], Zhengxu Huang[a], Junguo Dong[a], Mei Li[a], Wei Gao[b,c], Huiqing Nian[d], Zhong Fu[d], Guohua Zhang[b,c], Xinhui Bi[b], Ping Cheng[a], Zhen Zhou[a,*]

[a] School of Environmental and Chemical Engineering, Shanghai University, Shanghai 200444, China
[b] State Key Laboratory of Organic Geochemistry, Guangzhou Institute of Geochemistry, Chinese Academy of Sciences, Guangzhou 510640, China
[c] Graduate School of the Chinese Academy of Sciences, Beijing, China
[d] Hexin Analytical Instrument Co., Ltd., Guangdong, Guangzhou 510663, China

ARTICLE INFO

Article history:
Received 9 October 2010
Received in revised form 15 January 2011
Accepted 16 January 2011
Available online 26 January 2011

Keywords:
Aerosol
Aerodynamic lens
Single particle
Laser ionization
Bipolar time-of-flight mass spectrometer

ABSTRACT

This paper describes a new built single particle laser desorption/ionization time of flight mass spectrometer capable of determining the size and chemical compositions of individual aerosol particles in real-time. The instrument was compactly designed with bipolar grid reflectron mass analyzers for higher mass resolution. It measures 90 cm long × 70 cm wide × 170 cm high, weights ~170 kg and has a total power consumption of less than 2000 W. Standard polystyrene latex particles (PSL) and metallic solution were used to perform size and mass calibration, respectively, and the effect of inlet pressure of the aerodynamic lens on size calibration was also investigated. The instrument was first used for the ambient aerosol detection in Guangzhou City, China, and the preliminary measurements show its' ability to characterize the atmospheric aerosol particles containing different chemical compositions with diameters ranging from 250 to 2000 nm and a total hit rate above 30%. The preliminary measurements also show that the aerosol particles in Guangzhou, China can be mainly classified into five types, which are rich K, rich Na, Nark, carbonaceous, and metal containing, and their formations are also generally discussed.

1. Introduction

Atmospheric aerosols, ubiquitous in the air, have a rather wide size distribution ranging from less than 10 nm to more than 10 μm in diameter, and also a complex molecular constituent. Numerous studies have shown that their tremendous impacts on environment, climate and human health [1–3], and these effects have direct associations with the size and chemical compositions of the single particles [4–7]. For example, fine particles, having large surface-to-volume rate, can provide reaction sites for halogen-containing particles with poor reactivity in the stratosphere, and this process plays a vital role in stratospheric ozone depletion. In addition, epidemiological studies have shown that the decreased pulmonary function and respiratory is relevant to the increased levels of particulate matter, especially the particles less than 1 μm, because the fine particles can easily penetrate into the deepest of the lungs and cause damages. In order to better understand their various physical and chemical properties, as well as predicting their potential health and environmental effects, it is essential to obtain the two most important information of single aerosol particle: size and chemical compositions. To achieve these goals, great efforts have been made to develop more sophisticated analytical instruments in the past years [8].

Mass spectrometry based aerosol analysis techniques have been developed since from the seventies of the last century. Davis first used mass spectrometry to analyze particulate matter by impinging of particles on a heated filament and mass analyzed by a magnetic sector mass spectrometry [8]. However, this method gets no size information and only a single m/z can be analyzed per particle. LAMMA as a typical off-line method of particulate analysis was introduced in the 1970s. Though this method can provide single particle size and chemical compositions simultaneously, it has intrinsic shortcomings. Firstly, enough particles are needed to be collected on a substrate before analysis, so matrix effect is non-ignorable, and particles collected will suffer from physicochemical changes through evaporation, crystallization, and gas-solid conversion during prolonged periods of sampling and storage, especially for volatile and semi-volatile components. Secondly, this is a relative slow method of obtaining particle size, about 1 particle/min, thus it is difficult to get a statistical analysis conclusion in a short time. In 1984, Sinha [9] developed a method that could trace

* Corresponding author at: Institute of Environmental Pollution, & Health, Shanghai University, 99 Shangda Road, Shanghai, 200444 China. Fax: +86 20 32053571.
E-mail address: zhouzhen@shu.edu.cn (Z. Zhou).

1387-3806/$ – see front matter © 2011 Elsevier B.V. All rights reserved.
doi:10.1016/j.ijms.2011.01.017

individual particle in real time by using light scattering size measurement with exterior laser ablation. Here a quadrupole mass spectrometry was used and still only a single m/z could be analyzed per particle similar to magnetic mass spectrometry. Johnson and Murphy [10] further developed a method by replacing the quadrupole mass analyzer with a TOF mass analyzer which could obtain a complete mass spectrum per particle. Unfortunately, the size estimation based on the scattering intensity of the particles passing a single continuous laser is proved to be inaccurate. In 1994, Prather and co-workers [11] built an single particle time of flight mass spectrometry, shortly called ATOFMS, and the first transportable ATOFMS in 1997 that could precisely determine size and chemical compositions of single aerosol particles simultaneously and in real-time [12]. Now ATOFMS has been widely used especially after it was commercially available from TSI Corporation. Until now several other research groups have also developed their own single particle aerosol mass spectrometer [13–15].

China is a country that suffers from particulate pollution all the year, which is even heavier in Guangzhou when haze is severe from December to February [16,17]. It is impending to better understand the aerosol sources and actions in the atmosphere and offer reliable foundation for legislation. As a try to achieve these goals and combining with our experiences of developing high resolution time of flight mass spectrometry, we built a compact single particle laser desorption/ionization time of flight mass spectrometer called SPAMS. In this paper, the instrument's principle and design features as well as the preliminary experimental results are presented.

2. Instrumentation setup

The schematic diagram and photograph of the SPAMS are represented in Fig. 1. The entire instrument measures 90 cm long × 70 cm wide × 170 cm high, weights ~170 kg and has a total power consumption of 2000 W under sampling conditions. Common 220 V alternating current is enough for the entire instrument running which is especially helpful in field study.

Similar to other single particle instruments, it mainly consists of three parts: an aerodynamic lens for aerosol inlet, a two-laser beams system for particle sizing, and a bipolar time of flight mass spectrometry for the detection of the generated positive and negative ions. Aerosol particles are introduced into the aerodynamic lens through an electro-spark machined 80 μm critical orifice at a rate of ~75 ml/min. Aerodynamic lens serves as an interface to introduce aerosol particles from atmosphere into high vacuum to provide a collimated beam for succedent analysis. While exiting the aerodynamic lens, the particles gain a terminal velocity distribution, which is a function of their aerodynamic diameters during supersonic expansion. In the sizing region, every particle consecutively scatters two continuous laser beams with a space of 6 cm. In each scattering event, the scattered light is refocused and detected by a PMT (Model H6180-01, Hamamatsu, Japan). Once the signal from the PMT reaches the defined threshold, a TTL pulse is sent to the timing board. The time interval between the two pulses serves two functions: (1) the individual particle velocity is obtained, and from which the aerodynamic diameter of single particle is calculated. (2) The velocity calculated is used to precisely fire adsorption/ionization laser located 12 cm downside from the second laser beam when the particle reaches the center of the ion source. The generated positive and negative ions by the third laser are then detected by two microchannel plate (MCP) detectors, respectively. Signals from the two detectors are delivered to a 8 bit dual channel ADC data acquisition card (U1069A Agilent). Information including transit time, laser energy, hit or not, and ion signal intensity are recorded by homemade data acquisition software and stored in the computer.

2.1. Aerodynamic lens

The aerodynamic lens, first developed by Liu et al. [18], is capable of efficiently transmitting aerosol particles into the vacuum system in a wider size range, as well as providing even smaller particle beam divergence than traditional nozzle/skimmer inlet system [17]. For our instrument, it consists of six successive coaxial cylindrical orifices with decreasing diameters of 5.0, 4.8, 4.6, 4.3, 4.2, 4.0 mm and a 2.0 mm diameter exit nozzle, which can focus the particles onto the centerline of the orifices. The exit nozzle is also served to control the supersonic gas expansion, and it was proved that the particles velocity distribution during gas expansion is a function of their aerodynamic diameters. After exiting the aerodynamic lens, the particles pass through a 1 mm diameter flat skimmer into the sizing region, where the gas is pumped away by a 250 l/s turbo molecular pump. The distance between the bottom of the aerodynamic lens and the skimmer is optimized and fixed at 12 mm at last. The aerodynamic lens is mounted on a micromanipulator which helps to adjust the slight particle beam during alignment or after long distance transport. Eight locking screws are used to ensure its stability. It should be noted that the instrument was transported on a truck for in situ measurement two times due to experimental requirements, and there were no damage or readjustment needed.

2.2. Laser system

Most aerosol mass spectrometers use 532 nm Nd:YAG lasers for size determination because of their high scattering efficiency. In our instrument, two 75 mW continuous diode Nd:YAG lasers (MLL-III-532 CNI Changchun) operated at 532 nm are used as well. The two sizing lasers are aligned orthogonal to each other and perpendicular to the particle beam. Each laser beam is focused into a 300 μm spot located at the first focal point of the ellipsoidal mirror. When a particle comes through the laser spot, the generated scattering light is refocused to the ellipsoidal mirror's second focal point, where a shutter with a 2 mm aperture in the center is placed. The PMT is located 3 mm distance beyond the shutter, which greatly reduce the background noise and increase the receiving area of the PMT. Two beam dumps are used to absorb the surplus laser beam to reduce the background noise in the sizing region.

In the ionization region, a pulsed 266 nm Nd:YAG desorption/ionization laser (Ultra Quantel France) is used as a light source to ionize the particles. The laser pulse energy is adjustable from 0.1 mJ to 10 mJ, which can be continuously measured by an energy meter. For there is a time delay between the flash lamp trigger and the Q-switch, the timing circuit must make up the delay to guarantee the laser hitting the particle at the center of the ion source. For our system, the delay is 203 μs (Fig. 2). To improve the ionization efficiency, a focus lens with 20 cm focal length was used to focus the laser beam into a 300 μm spot. By adjusting two whole-reflect lens, the laser beam direction can be translated up and down or sideways and the laser focal spot can also be fine tuned using the precise translation stages.

2.3. Bipolar time of flight mass spectrometer

Unlike ATOFMS's coaxial reflectrons [19], a z-shaped bipolar time of flight mass spectrometer is used to simultaneously detect the positive and negative ions generated by laser ionization. The gridded design was adopted in our bipolar mass analyzers, and each analyzer has four set of mesh grids with ion transmission rate of 90% as shown in Fig. 1a. Although this design reduces the sensitivity, it is easier to adjust and obtain higher resolution than gridless design [20]. In order to reduce the ion losses due to ion beam divergence, an einzel lens is used in the accelera-

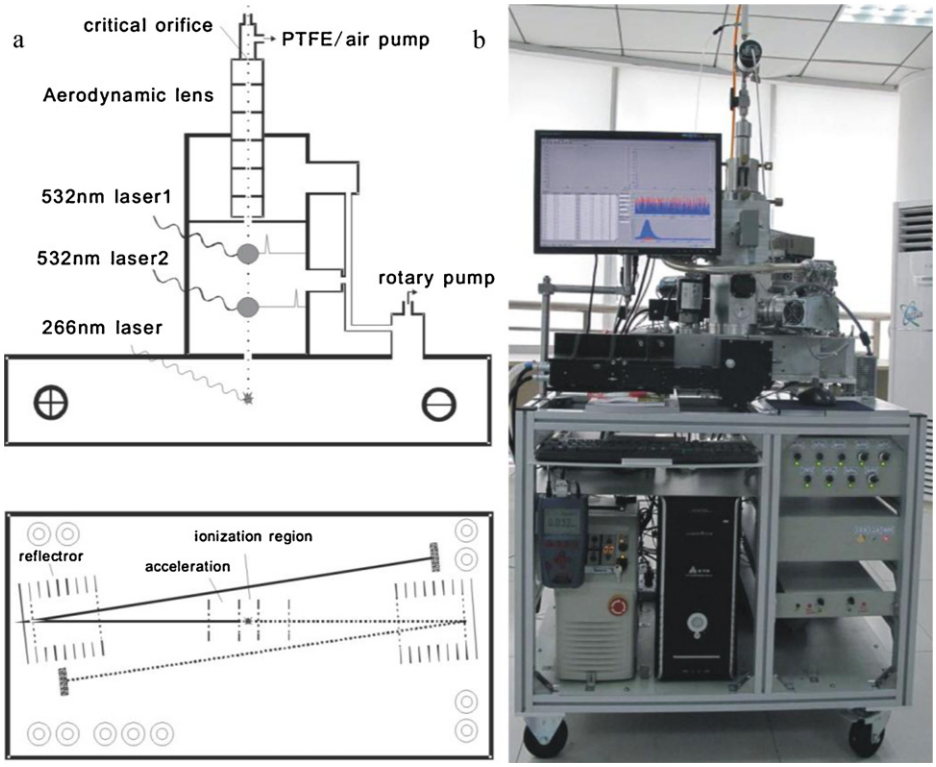

Fig. 1. (a) Schematic diagram of the SPAMS; (b) photograph of the SPAMS.

tion region. Here, the theoretical voltages were calculated using matlab7.0 and ion trajectories simulated using simion7.0 program. Practical values were later adjusted on the basis of experimental measurements. The source configuration has a 2600 V drawout potential over a 0.5 cm source region and a 3000 V, 3.4 cm acceleration region. The field free region is 46 cm long and floating at 3000 V, and the ions have a total fight path of 70 cm and a reflection angle of 4.5°. The voltages used for the positive and negative ion modes are the same except that, in positive ion mode, the MCP is floated at −3000 V acceleration voltage, while in negative, an additional 1700 V is superposed on the +3000 V acceleration voltage. Divider resistors are used to keep each microchannel plate at a voltage of ~800 V. Due to imperfect spatial dispersion compensation from particle to particle, high voltage fluctuation, mechanical machining and the assembling accuracy, time of flight variations from particle to particle exist. Since an integer mass number is adopted when the peak error is varied within ±0.5 amu to the integer, the particle variations in our SPAMS can be ignored since the variations are always within ±0.3 amu in the mass range of 500 amu.

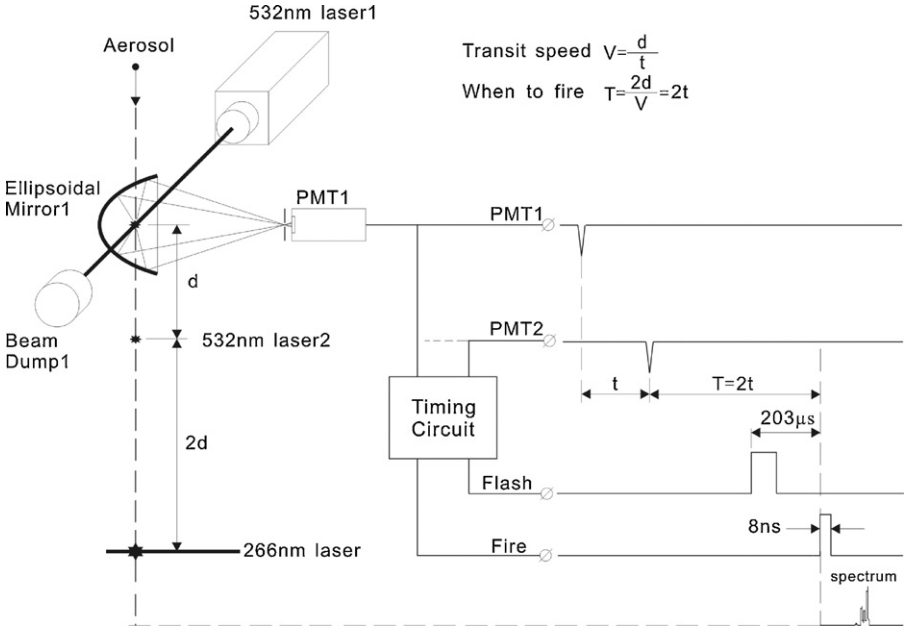

Fig. 2. Timing and pulse scheme for the sizing, laser ionization and detection system.

2.4. Vacuum structure optimization

Vacuum structure of the instrument was simplified compared with ATOFMS and A-ATOFMS [21]. The whole pumping system includes only three turbo molecular pumps and a rotary vane vacuum pump used as backing pump of the whole pumping system. This configuration reduces the cost, power consumption and weight of the instrument. A 250 l/s turbo molecular pump (Turbo-V 301 Varian Inc.), 70 l/s turbo molecular pump (Turbo-V 80 Varian Inc.) and 250 l/s split-flow turbo molecular pump (Turbo-V301SF Varian Inc.) are located in the differential pumping region, the sizing region and the mass spectrometer region, respectively. The split-flow pump with a pumping speed of 11 l/s on the V301SF is used to back the 70 l/s pump in the sizing region as well as the 250 l/s pump in the differential pumping region. The split-flow pump is, in turn, backed by a 6 l/min rotary vane vacuum pump (DS-402 Varian Inc.) with oil vapour sorption trap, which effectively avoids the oil vapour contamination [13]. This pumping scheme yields a pressure of ~2 Torr at the entrance to the aerodynamic lens, 3×10^{-3} Torr in the differential pumping region, 5×10^{-5} Torr in the sizing region and 7×10^{-7} Torr in the mass spectrometer region. Pressure measurements are accomplished using a pirani gauge, an active rough vacuum gauge and two cold cathode ionization gauges corresponding to the described four regions.

2.5. Aerosol particle size and mass calibration

For our instrument, the standard PSL particles of known size were used for aerosol particle size calibration, and the metallic solution containing known metal ions was used for mass calibration. The PSL particles we used are in the size of 300 nm, 500 nm, 720 nm, 1 μm and 2 μm in diameter, and the nominal ions dissolved in the solution are Li, Na, K, V, Ba, and Pb. Each time a drop of PSL suspension or metallic solution is dissolved in 50 ml ultra pure deionized water, and atomized by a single-jet aerosol generator (TSI 9302, USA). The generated aerosol spray passes through a Nafion dryer (Model MD-070, PERMAPURE, USA) followed by a 50 cm homemade silica gel diffusion dryer with the humidity reducing from 86% to 17%, which is necessary for aerosol inlet. Then the dried aerosol controlled by a rotor flowmeter with ~75 ml/min flow enters into the aerodynamic lens through an 80 μm critical orifice. In our experiment, the aerosol inlet tube was machined into a three branch structure. The top vent was for aerosol sampling, and the side one connected to the atmosphere using a PTFE membrane.

The transit times of different particles between the two laser beams are a function of their aerodynamic diameters. Thus the obtained transit times can convert to their aerodynamic diameters using a size calibration curve. Fig. 3 shows the transit times of five sizes of PSL particles at the inlet pressure of 1.956 Torr, and the curve with round dots in Fig. 4 is the corresponding plot with a first-order exponential fitting in the form of $y = A1 \times \exp(-x/t1) + y0$, where $A1 = 0.00747$, $t1 = -163.46064$, $y0 = 0.09511$, and $R^2 = 0.99946$. Since aerodynamic lens is sensitive to the pressure changes at the inlet orifice, the slight changes in inlet pressure will affect the focusing properties of the particles which then lead to a shift in calibration curve [14]. Detailed effects of the inlet pressure on calibration curves were investigated by changing the size of the critical orifice. Every time, particle velocities with the same diameter were measured at six different inlet pressures. Then the velocities of five different particles versus their aerodynamic diameters were plotted. Fig. 4 shows the six calibration curves at different inlet pressures. The transit time of the particle increases with the inlet pressure of aerodynamic lens going down, and this is due to the less gas-particles collisions thus smaller velocity during the supersonic expansion in low inlet pressure. In Fig. 4, it is clear to see that even though the pressure change is small, for example,

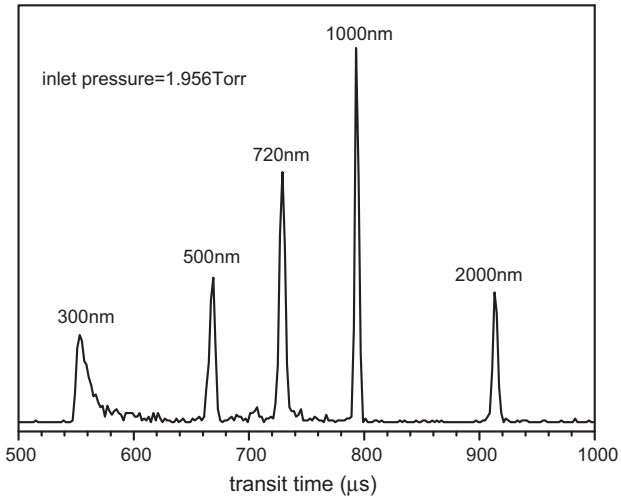

Fig. 3. Transit times for five different kinds of PSL particles at inlet pressure of 1.956 Torr.

from 2.440 Torr to 2.505 Torr, the calibration curve variation is still discernible. So the inlet pressure was continuously monitored in case that the critical orifice was partially blocked by contamination during experiments, and the regular cleaning is needed to keep the inlet pressure constant.

The mass calibration was performed by using the following equation:

$$\frac{m}{z} = (at + b)^2$$

where a represents the slope of the linear function in the brackets and b the intercept. In the experiment, not all the ion species appear in every mass spectrum, and some ion species may appear in one spectrum and may not in another. Therefore, the ion peaks used for calibration must be chosen from different mass spectra. Though different particles are fired at different positions in the laser beam, the particle to particle variations in time of flight is unavoidable which will result in errors in mass calibration curve [22]. An alternative method is that, for the same m/z, several different time-of-flight values are chosen, and only the average value is used for mass calibration.

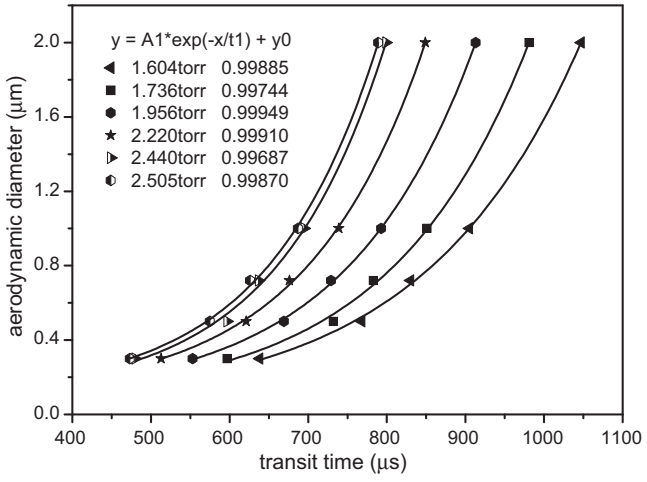

Fig. 4. Corresponding size calibration curves at seven different inlet pressures.

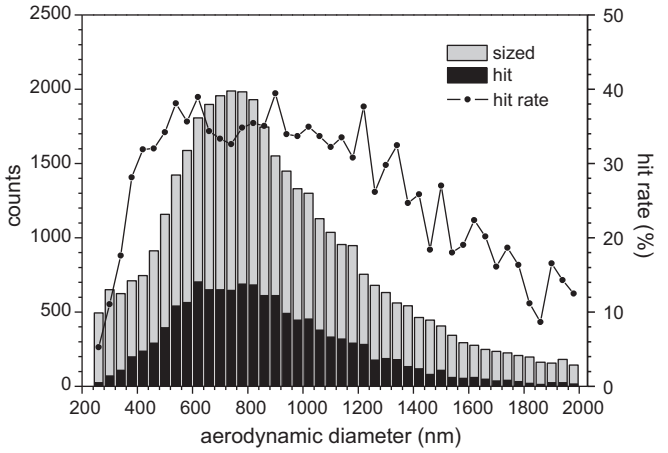

Fig. 5. Hit rate and the number distribution of sized and detected ambient particles.

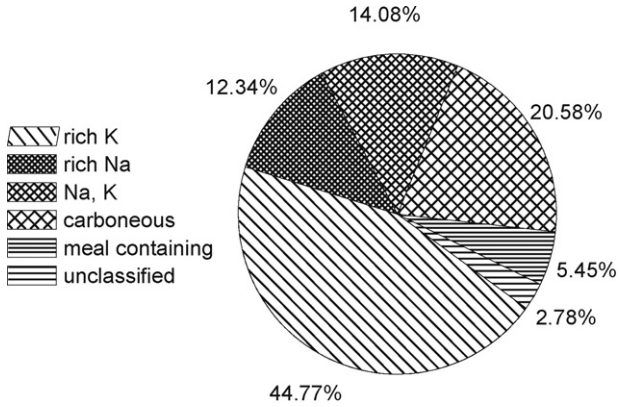

Fig. 6. Chemical composition and proportional distribution of the different types ambient particles

3. Ambient aerosol measurement

Outdoor ambient particles were initially used to evaluate the performance of the instrument. The ambient particles were sampled by a 5 l/min sucking pump connected to the side vent of the inlet tube. A static-free silicone tube or copper pipe was attached to the top of the inlet. Due to the limitation of the maximum repletion rate of the 266 nm Nd:YAG laser, the sizing rate was adjusted to be less than 20 particles/s. Ambient aerosol flow was diluted by a factor depending on the number concentration of the ambient particles. The SPAMS was located in a building of the Science City, Guangzhou China. This site is nearby residential, traffic, industrial and construction emissions sources and basically represents a suburb area. Aerosol particles were sampled into SPAMS through a 6 m long copper tube out of the window. The inlet of the sampling tube is about 10 m above the ground. The ionization laser energy is 0.6 mJ per pulse. It is noteworthy that the actual ionization energy may be slightly larger because of the energy loss after laser beam passing the glass window. A particle was considered detected and its mass spectrum is saved whenever the signal intensity from either the positive or the negative ion detector exceeded 5 V. During a 90 min measurement, a total of 37,612 particles were sized and 12,378 chemically analyzed with diameters ranging from 250 to 2000 nm, 12,947 particles produced both positive and negative ion spectra and the average hit rate of 32.3% was obtained. Fig. 6 is a plot of the measured aerodynamic diameters of the detected particles and also the hit rate variation with the particle's aerodynamic diameter. The aerodynamic diameters were calculated using the calibration curve at the pressure of 1.956 Torr. The gray histogram is the plot of particles sized, and the dark histogram is that particles chemically analyzed. As shown in Fig. 5, particles were detected and chemically analyzed from 250 to 2000 nm, peaking at about 700 nm. The hit rate was approximately uniform for particles from ~400 to ~1200 nm, about 33%, while it decreased rapidly from less than 400 nm and lager than 1200 nm. This size-dependent hit rate is due to the different scattering intensity between large and small particles [23]. Since large particles scatter more light than small particles, they tend to reach the trigger threshold earlier than small particles. The distance from the center of the second green laser to the center of the ion source is consistent. So, if hit rate for a given range is optimized, ionization laser will fire earlier for larger particles and later for smaller particles.

The particles detected by SPAMS can be analyzed using ART-2a algorithm based single particle analysis software toolkit known as YAADA2.0 (www.yaada.org) [24], which has been widely used for ATOFMS data analysis [25–27]. The ART-2a algorithm and its use for single particle characterization is described in detail elsewhere [28]. The ART-2a parameters used in this study were a learning rate of 0.05, vigilance factor of 0.5, and 20 iterations. The 12,947 particles were classified into 306 clusters based on the similarity of positive ion spectra. 80% of the analyzed particles were accounted for by the top 10 clusters, 93% by the top 20 clusters, and 97% by the top 32 clusters. While the top 32 clusters were further grouped by hand into five general particle types based on the major ion peaks in the mass spectra, i.e., rich K, rich Na, Nark, carbonaceous, and metal containing. Fig. 6 is the chemical composition and proportional distribution of the different types ambient particles. The spectra shown in Fig. 7 are the corresponding average spectra to the five particle types. During this ambient measurement, K^+, sulfate, and nitrate were detected in most of the particles, and about 85% of the total positive spectra contained K^+, 72% negative spectra contained sulfate, and over 90% negative spectra contained nitrate. In rich K type, as shown in Fig. 7a, $^{39}K^+$ is far larger than other peaks in the positive ion mass spectrum, NO_2^- and NO_3^- and HSO_4^- are the strongest peaks in the negative spectrum. Alkali metal ions are very sensitive to laser aerosol mass spectrometer [29], and online studies have shown that K^+ is a reliable signature for the identification of biomass particles [30,31]. These rich K particles may result

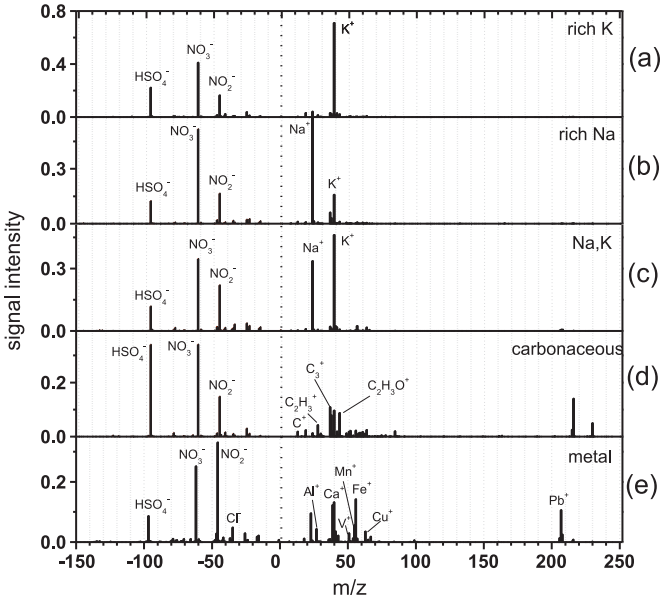

Fig. 7. Average mass spectra of the five grouped particle types.

from biomass combustion as raw mass spectra show that many rich K particles have levoglucosan negative ion fragments at −45, −59, and −73, while levoglucosan was considered as the biomass burning tracers in other biomass characterization studies [32–34]. In Fig. 7b, Na^+ is the strongest peak in the positive mass spectrum, the negative spectrum are very similar to rich K and Na + K types. Sea salt is the primary source of Na^+ in the ambient aerosols. Moreover, biomass burning and soil are the main sources of Na^+ as well [30,35]. Strong nitrate (NO_2^- and NO_3^-), indicates a significant amount of aged process of these rich Na particles. Na + K particles may result from biomass burning or the condensation between rich K and rich Na particles. Fig. 7d shows the mass spectrum of carbonaceous particle type. Organic carbon particle (OC) and elemental carbon (EC) particles are the two common carbonaceous particles that we observed. The number considered as OC and EC particles are 1376 and 466, respectively. This result agrees well with the previous study where OC was considered the major contribution to PM2.5 in haze days in Guangzhou [17]. It is notable that about 0.5% organic amine particles, 1% environmental tobacco particles, 5% high molecular organic particles were grouped into carbonaceous particle type. Detailed characterization of carbonaceous particle type in Guangzhou will be pressed in other studies. Fig. 7e is the average spectrum of the containing metal particles, several metals were detected including Li^+, Mg^+, Al^+, Ca^+, V^+, Mn^+, Fe^+, Cu^+, Zn^+, Sn^+, Ba^+, Pb^+, etc. Particles from different sources may have different metal types. These metal containing particles have various sources in other ATOFMS studies. Particles containing Li^+, Al^+, Ca^+, Fe^+, etc. in the positive spectra together with some special ions in the negative ions such as AlO_2^-, PO_2^-, SiO_3^-, PO_3^- were detected in suspended soil [35]. V^+ and VO^+ were detected from the emissions of heavy oil combustion such as industrial boilers, ships and power plants residual fly ash [36–38]. Particles containing Pb^+, Cu^+, Zn^+, Cl^- may from the waste incineration and industrial emissions [39,40]. Detailed characterization of ambient trace metals will be discussed in further studies.

4. Conclusion

We presented a new built single particle laser desorption/ionization time of flight mass spectrometer capable of determining the size and chemical compositions of individual aerosol particles in real-time. The instrument was compactly designed with bipolar grid reflectron mass analyzers for higher mass resolution, an aerodynamic lens for high efficient particle inlet, and a laser system for precisely sizing and ionization. The ambient measurement in Guangzhou, China shows that SPAMS can rapidly characterize the atmospheric aerosol particles containing various chemical compositions with diameters ranging from 250 to 2000 nm and a total hit rate above 30%. ART-2a based single particles analysis method manifests its practical ability in atmospheric aerosol researches. The preliminary measurements also show that the aerosol particles in Guangzhou, China could be mainly classified into five types, which are rich K, rich Na, Nark, carbonaceous, and metal containing, and their formations are also generally discussed.

Acknowledgements

The authors gratefully acknowledge the assistance of Yerong Zhang in machining and alignment of the instrument. We also express pure-hearted appreciation to Youbo Dong, Shaode Chen, and Yaoli Li for their help in developing circuit and software, respectively. This work was supported by National High-Tech Research and Development Program of China (2006AA06Z425), Shanghai Leading Academic Discipline Project (No. S30109) and the Innovation Fund from Shanghai University (A.10-0111-09-010).

Appendix A. Supplementary data

Supplementary data associated with this article can be found, in the online version, at doi:10.1016/j.ijms.2011.01.017.

References

[1] P.R. Buseck, M. Posfai, Airborne minerals and related aerosol particles: effects on climate and the environment, Proc. Natl. Acad. Sci. U.S.A. 96 (1999) 3372–3379.
[2] T.L. Anderson, R.J. Charlson, S.E. Schwartz, R. Knutti, O. Boucher, H. Rodhe, J. Heintzenberg, Climate forcing by aerosols: a hazy picture, Science 300 (2003) 1103–1104.
[3] C.A. Pope, Particulate pollution and health: a review of the Utah Valley experience, J. Expo. Anal. Environ. Epidemiol. 6 (1996) 23–34.
[4] B.D. Horne, D.G. Renlund, A.G. Kfoury, H.T. May, C.A. Pope, Heart failure exacerbation and exposure to fine particulate air pollution, Circulation 118 (2008) S796.
[5] C.A. Pope, M. Ezzati, D.W. Dockery, Fine-particulate air pollution and life expectancy in the United States, N. Engl. J. Med. 360 (2009) 376–386.
[6] C.A. Pope, Mortality from copper smelter emissions: Pope responds, Environ. Health Perspect. 115 (2007) A439–A440.
[7] S. Solomon, R.W. Portmann, R.R. Garcia, L.W. Thomason, L.R. Poole, M.P. McCormick, The role of aerosol variations in anthropogenic ozone depletion at northern midlatitudes, J. Geophys. Res. Atmos. 101 (1996) 6713–6727.
[8] W.D. Davis, Abstract: surface ionization mass spectroscopy of airbone particulates, J. Vacuum Sci. Technol. 10 (1973) 278.
[9] M.P. Sinha, R.M. Platz, V.L. Vilker, S.K. Friedlander, Analysis of individual biological particles by mass-spectrometry, Int. J. Mass Spectrom. Ion Process. 57 (1984) 125–133.
[10] P.J. Mckeown, M.V. Johnston, D.M. Murphy, Online single-particle analysis by laser desorption mass-spectrometry, Anal. Chem. 63 (1991) 2069–2073.
[11] K.A. Prather, T. Nordmeyer, K. Salt, Real-time characterization of individual aerosol-particles using time-of-flight mass-spectrometry, Anal. Chem. 66 (1994) 1403–1407.
[12] E. Gard, J.E. Mayer, B.D. Morrical, T. Dienes, D.P. Fergenson, K.A. Prather, Real-time analysis of individual atmospheric aerosol particles: design and performance of a portable ATOFMS, Anal. Chem. 69 (1997) 4083–4091.
[13] D.A. Lake, M.P. Tolocka, M.V. Johnston, A.S. Wexler, Mass spectrometry of individual particles between 50 and 750 nm in diameter at the Baltimore supersite, Environ. Sci. Technol. 37 (2003) 3268–3274.
[14] A. Zelenyuk, D. Imre, Single particle laser ablation time-of-flight mass spectrometer: an introduction to SPLAT, Aerosol Sci. Technol. 39 (2005) 554–568.
[15] D.S. Thomson, M.E. Schein, D.M. Murphy, Particle analysis by laser mass spectrometry WB-57F instrument overview, Aerosol Sci. Technol. 33 (2000) 153–169.
[16] X.X. Tie, J.J. Cao, Aerosol pollution in China: present and future impact on environment, Particuology 7 (2009) 426–431.
[17] J.-H. Tan, J.-C. Duan, D.-H. Chen, X.-H. Wang, S.-J. Guo, X.-H. Bi, G.-Y. Sheng, K.-B. He, J.-M. Fu, Chemical characteristics of haze during summer and winter in Guangzhou, Atmos. Res. 94 (2009) 238–245.
[18] P. Liu, P.J. Ziemann, D.B. Kittelson, P.H. Mcmurry, Generating particle beams of controlled dimensions and divergence. 1. Theory of particle motion in aerodynamic lenses and nozzle expansions, Aerosol Sci. Technol. 22 (1995) 293–313.
[19] Y.X. Su, M.F. Sipin, H. Furutani, K.A. Prather, Development and characterization of an aerosol time-of-flight mass spectrometer with increased detection efficiency, Anal. Chem. 76 (2004) 712–719.
[20] R.P. Schmid, C. Weickhardt, Designing reflectron time-of-flight mass spectrometers with and without grids: a direct comparison, Int. J. Mass Spectrom. 206 (2001) 181–190.
[21] K.A. Pratt, J.E. Mayer, J.C. Holecek, R.C. Moffet, R.O. Sanchez, T.P. Rebotier, H. Furutani, M. Gonin, K. Fuhrer, Y. Su, S. Guazzotti, K.A. Prather, Development and characterization of an aircraft aerosol time-of-flight mass spectrometer, Anal. Chem. (2009).
[22] P.G. Carson, K.R. Neubauer, M.V. Johnston, A.S. Wexler, Online chemical-analysis of aerosols by rapid single-particle mass-spectrometry, J. Aerosol Sci. 26 (1995) 535–545.
[23] A. Zelenyuk, J. Yang, D. Imre, E. Choi, Achieving size independent hit-rate in single particle mass spectrometry, Aerosol Sci. Technol. 43 (2009) 305–310.
[24] J.O. Allen, YAADA: Software Toolkit to Analyze Single-Particle Mass Spectral Data, 2005.
[25] S.H. Pastor, J.O. Allen, L.S. Hughes, P. Bhave, G.R. Cass, K.A. Prather, Ambient single particle analysis in Riverside, California by aerosol time-of-flight mass spectrometry during the SCOS97-NARSTO, Atmos. Environ. 37 (2003) S239–S258.
[26] R.C. Moffet, B. de Foy, L.T. Molina, M.J. Molina, K.A. Prather, Measurement of ambient aerosols in northern Mexico City by single particle mass spectrometry, Atmos. Chem. Phys. 8 (2008) 4499–4516.
[27] S.M. Toner, L.G. Shields, D.A. Sodeman, K.A. Prather, Using mass spectral source signatures to apportion exhaust particles from gasoline and diesel powered vehicles in a freeway study using UF-ATOFMS, Atmos. Environ. 42 (2008) 568–581.

[28] X.H. Song, P.K. Hopke, D.P. Fergenson, K.A. Prather, Classification of single particles analyzed by ATOFMS using an artificial neural network, ART-2A, Anal. Chem. 71 (1999) 860–865.
[29] D.S. Gross, M.E. Galli, P.J. Silva, K.A. Prather, Relative sensitivity factors for alkali metal and ammonium cations in single-particle aerosol time-of-flight mass spectra, Anal. Chem. 72 (2000) 416–422.
[30] P.J. Silva, D.Y. Liu, C.A. Noble, K.A. Prather, Size and chemical characterization of individual particles resulting from biomass burning of local Southern California species, Environ. Sci. Technol. 33 (1999) 3068–3076.
[31] S.A. Guazzotti, D.T. Suess, K.R. Coffee, P.K. Quinn, T.S. Bates, A. Wisthaler, A. Hansel, W.P. Ball, R.R. Dickerson, C. Neususs, P.J. Crutzen, K.A. Prather, Characterization of carbonaceous aerosols outflow from India and Arabia: biomass/biofuel burning and fossil fuel combustion, J. Geophys. Res. Atmos. 108 (2003).
[32] Z.S. Zhang, G. Engling, C.Y. Lin, C.C.K. Chou, S.C.C. Lung, S.Y. Chang, S.J. Fan, C.Y. Chan, Y.H. Zhang, Chemical speciation, transport and contribution of biomass burning smoke to ambient aerosol in Guangzhou, a mega city of China, Atmos. Environ. 44 (2010) 3187–3195.
[33] T Zhang, M. Claeys, H. Cachier, S.P. Dong, W. Wang, W. Maenhaut, X.D. Liu, Identification and estimation of the biomass burning contribution to Beijing aerosol using levoglucosan as a molecular marker, Atmos. Environ. 42 (2008) 7013–7021.
[34] B.R.T. Simoneit, J.J. Schauer, C.G. Nolte, D.R. Oros, V.O. Elias, M.P. Fraser, W.F. Rogge, G.R. Cass, Levoglucosan, a tracer for cellulose in biomass burning and atmospheric particles, Atmos. Environ. 33 (1999) 173–182.
[35] P.J Silva, R.A. Carlin, K.A. Prather, Single particle analysis of suspended soil dust from Southern California, Atmos. Environ. 34 (2000) 1811–1820.
[36] D.A. Figueroa, C.J. Rodriguez-Sierra, B.D. Jimenez-Velez, Concentrations of Ni and V, other heavy metals, arsenic, elemental and organic carbon in atmospheric fine particles (PM2.5) from Puerto Rico, Toxicol. Ind. Health 22 (2006) 87–99.
[37] H.N Jang, Y.C. Seo, J.H. Lee, K.W. Hwang, J.I. Yoo, C.H. Sok, S.H. Kim, Formation of fine particles enriched by V and Ni from heavy oil combustion: anthropogenic sources and drop-tube furnace experiments, Atmos. Environ. 41 (2007) 1053–1063.
[38] Z.Q. Xie, L.G. Sun, J.D. Blum, Y.Y. Huang, W. He, Summertime aerosol chemical components in the marine boundary layer of the Arctic Ocean, J. Geophys. Res. Atmos. 111 (2006).
[39] R.C. Moffet, Y. Desyaterik, R.J. Hopkins, A.V. Tivanski, M.K. Gilles, Y. Wang, V. Shutthanandan, L.T. Molina, R.G. Abraham, K.S. Johnson, V. Mugica, M.J. Molina, A. Laskin, K.A. Prather, Characterization of aerosols containing Zn, Pb, and Cl from an industrial region of Mexico City, Environ. Sci. Technol. 42 (2008) 7091–7097.
[40] Y. Zhang, X. Wang, H. Chen, X. Yang, J. Chen, J.O. Allen, Source apportionment of lead-containing aerosol particles in Shanghai using single particle mass spectrometry, Chemosphere 74 (2009) 501–507.